ORGANIC CHEMISTRY

Helicity-modulated remote C-H functionalization

Na Yang[1], Chengshuo Shen[2]*, Guoli Zhang[1], Fuwei Gan[1], Yongle Ding[1], Jeanne Crassous[3], Huibin Qiu[1]*

Remote C-H functionalization is highly important for the conversion and utilization of arenes, but the conventional routes are comprehensively developed with the assistance of transition metal catalysts or templates. We report a facile metal/template-free electrochemical strategy for remote C-H functionalization in a helical system, where aromatic or aliphatic hydrogen act as a directing group to promote the alkoxylation at the opposite site of the helical skeleton by generating a unique helical "back-biting" environment. Such helicity-modulated C-H functionalization is prevalent for carbo[*n*]helicenes (*n* = 6 to 9, primitive or substituted) and hetero[6]helicenes and also occurs when the aryl hydrogen on the first position is replaced by a methyl group or a phenyl group. Thus, the relatively inert helicene skeleton can be precisely furnished with a rich array of alkoxy pendants with tunable functional moieties. Notably, the selective decoration of a methoxy group on *N*-methylated aza[6]helicene close or distant to the nitrogen atom leads to distinct luminescence variation upon changing the solvents.

INTRODUCTION

Direct functionalization of C-H bond provides an efficient route to create various complex molecules (*1–4*). Among them, regioselective C-H functionalization of arenes improves the utilization of substrates and substantially reduces the posttreatment complexity (*5, 6*). For instance, classical electrophilic aromatic substitution (S$_E$Ar) and Friedel-Crafts reactions have been widely used to prepare substituted arenes, where the electronic nature of arenes regulates the selectivity (*7–9*). On the other hand, transition metal–promoted C-H activation assisted by directing groups has enabled a tremendous diversity of decorated arenes. Because Ackermann's group (*10*) first reported the meta-alkylated product of Ru-catalyzed C-H activation, major advances in distal C-H functionalization catalyzed by transition metals have been witnessed. By constructing appropriate five- or six-membered cyclic intermediates with the metal center, regioselective functionalization of *meta*- or *para*-C-H bonds can be precisely achieved (Fig. 1A, i) (*11–15*). As an extension, remote C-H activation directed by templates has been recently developed to override the intrinsic electronic or steric biases in arenes (Fig. 1A, ii) (*16–18*). This normally involves the formation of a macrocyclic pretransition state to activate the desired more distal C-H bonds. Noncovalent interactions have also been developed as drivers in remote C-H functionalization to manipulate the regioselectivity. Kuninobu and co-workers (*19*) used hydrogen bonding between the substrate and catalyst to control the regioselectivity of C-H borylation (Fig. 1A, iii). In 2017, Zhang and co-workers (*20*) pioneered a bifunctional template-mediated approach for remote C-H olefination of heteroarenes (Fig. 1A, iv). Maiti's group subsequently explored the potential generality of the bifunctional template-mediated C-H functionalization of nitrogen-fused heterocycles on a distal site (Fig. 1A, iv) (*21*). Compared with simple arenes, regioselective remote C-H functionalization of polycyclic aromatic hydrocarbons (PAHs) that have extended π-conjugated systems is more difficult because of the multiple similar sp^2 C-H bonds (*22–24*), and remote functionalization of nonplanar PAHs with reduced symmetry encountered more challenges.

Here, we develop a facile helicity-modulated approach for remote C-H functionalization of nonplanar helical PAHs (*25–27*) in the absence of transition metal catalyst or template (Fig. 1B). Electrochemistry (*28–36*) was used to activate the helical substrates (*37–39*), and alkoxylation was simultaneously conducted under mild conditions. It was found that the first-position aryl hydrogen H$_{A1}$ of the helical skeleton acted as a directing group to promote the remote alkoxylation by generating a unique "back-biting" environment. Likewise, when H$_{A1}$ was replaced by a methyl group or a phenyl group, the aliphatic or aromatic hydrogen on the substituent group can form a similar back-biting pattern to direct the remote C-H functionalization. Such helicity-modulated back-biting effect is systematically verified by a rich array of helicenes and substituted helicenes together with single-crystal analysis and theoretical calculations. This strategy provides a distinctive pathway for accurate remote C-H functionalization of helical PAHs, following the previous advances in late-stage (*40, 41*) and photochemical functionalization (*42*).
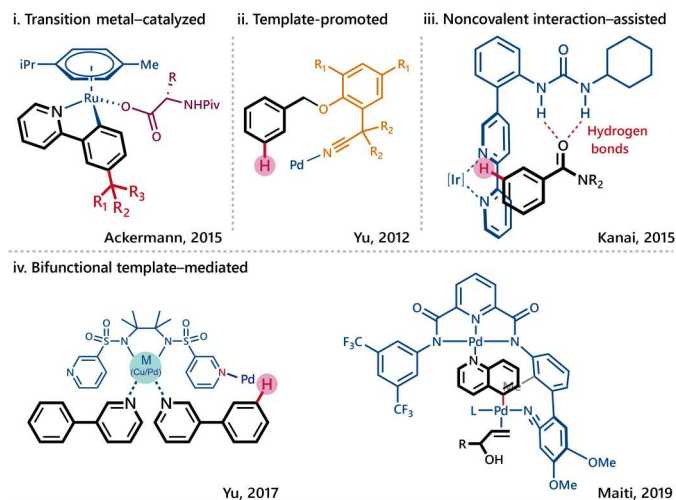
RESULTS AND DISCUSSION

We first screened the reaction conditions by choosing carbo[6]helicene **6H** and methanol (MeOH) as the model substrates (Table 1). By adopting 2 eq. of ^{n}Bu$_4$NBr and 0.1 M ^{n}Bu$_4$NBF$_4$ with acetonitrile (MeCN) as the solvent in an undivided cell (constant current = 5 mA), a mono-methoxy-substituted product **6H-OMe** (**1**) was obtained as the only alkoxylated product with a yield of 85%. Nuclear magnetic resonance (NMR) and single-crystal x-ray diffraction revealed that a methoxy group was substituted on position-E1 of **6H** (figs. S21 to S26 and S89). When ^{n}Bu$_4$NBr was removed, no methoxylation was detected, and **6H** was transformed into a mixture of unidentifiable overoxidized products (entry 2). Replacing ^{n}Bu$_4$NBr by ^{n}Bu$_4$NCl or ^{n}Bu$_4$NI also resulted in a failure of methoxylation (entries 3 and 4; for ^{n}Bu$_4$NCl, a mixture of

[1]School of Chemistry and Chemical Engineering, Zhangjiang Institute for Advanced Study, Frontiers Science Center for Transformative Molecules, State Key Laboratory of Metal Matrix Composites, Shanghai Jiao Tong University, Shanghai 200240, China. [2]Department of Chemistry, Key Laboratory of Surface & Interface Science of Polymer Materials of Zhejiang Province, Zhejiang Sci-Tech University, Hangzhou 310018, China. [3]Institut des Sciences Chimiques de Rennes, Université de Rennes, UMR CNRS 6226, Campus de Beaulieu, Rennes 35042, France.
*Corresponding author. Email: hbqiu@sjtu.edu.cn (H.Q.); shenchengshuo@zstu.edu.cn (C.S.)

A Conventional remote C-H functionalization

i. Transition metal–catalyzed

Ackermann, 2015

ii. Template-promoted

Yu, 2012

iii. Noncovalent interaction–assisted

Hydrogen bonds

Kanai, 2015

iv. Bifunctional template–mediated

Yu, 2017

Maiti, 2019

B Helicity-modulated hydrogen-directed remote C-H functionalization (this work)

nH
(n = 6 ~ 9)

+ ROH

Undivided cell
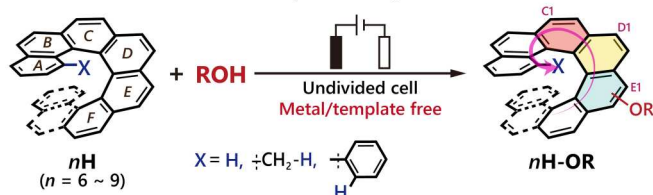Metal/template free

nH-OR

X = H, ÷CH₂-H,

Fig. 1. Methods for remote C-H functionalization of arenes.

unconverted **6H** and some randomly chlorinated [6]helicene was eventually found; for ^{n}Bu₄NI, the **6H** precursor was hardly converted to **6H-OMe**). The yield of **6H-OMe** (**1**) obviously decreased when less ^{n}Bu₄NBr was adopted (entries 5 and 6), and increasing the feed of ^{n}Bu₄NBr also slightly reduced the yield of **6H-OMe** (**1**) (entries 7 to 9). When the current of the electrochemical alkoxylation was decreased to 2 mA, the yield of **6H-OMe** (**1**) decreased to 55% with a considerable amount of untransformed **6H** (entry 10). On the other hand, increasing the current to 8 mA led to a 60% yield of **6H-OMe** (**1**) along with unidentifiable overoxidized products (entry 11). The reaction cannot proceed without electricity (entry 12), implying that the C-H functionalization underwent an electro-oxidative process.

We subsequently used a variety of other alcohols to evaluate the compatibility of the electrochemical C-H functionalization (Fig. 2A). The alkoxylation again precisely occurred on position-E1 of **6H** when primary, secondary, and tertiary alcohols were introduced. Ethanol, sterically hindered isopropanol and tertiary butanol, and long-chain n-hexanol afforded the alkoxylated products (**2** to **5**) in 56 to 78% isolated yields. Cyclohexanol and benzyl alcohols gave the corresponding products **6** and **7** in 55 and 62% yields, respectively. **6H** could also be decorated with functional hydroxyethoxy and bromoethoxy groups in 67 and 70% isolated yields (**8** and **9**). Note that the electrochemical functionalization was inaccessible with the addition of primary and secondary amines, thiols, and carboxylic acids under the standard condition, indicating a unique selection of the nucleophiles.

Table 1. Optimization of reaction conditions for electrochemical methoxylation of 6H. Standard condition: undivided cell, **6H** (0.1 mmol), MeOH (10 eq.), ^{n}Bu₄NBr (2 eq.), ^{n}Bu₄NBF₄ (0.1 M), MeCN (10 ml), 25°C, 12 hours, graphite electrode, and constant current electrolysis at 5 mA. For clarity, the aromatic rings of carbo[6]helicene are labeled by capital characters, and the C-H bonds are labeled by Arabic numbers.
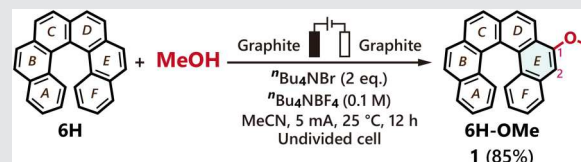
Entry	Deviation from standard condition	Yield[†]
1	None	85%
2	^{n}Bu₄NBr: 0 eq.	0%
3	^{n}Bu₄NBr: 0 eq.; ^{n}Bu₄NCl: 2 eq.	Trace
4	^{n}Bu₄NBr: 0 eq.; ^{n}Bu₄NI: 2 eq.	0%
5	^{n}Bu₄NBr: 0.2 eq.	20%
6	^{n}Bu₄NBr: 0.5 eq.	45%
7	^{n}Bu₄NBr: 5 eq.	80%
8	^{n}Bu₄NBr: 10 eq.	72%
9	^{n}Bu₄NBr: 0.1 M; ^{n}Bu₄NBF₄: 0 M	65%
10	2 mA	55%
11	8 mA	60%
12	0 mA	0%

[†]Yields are for isolated products.

Substituted carbo[6]helicene was also surveyed to further investigate the electrochemical C-H functionalization (Fig. 2B). Asymmetric monosubstituted carbo[6]helicenes including 2-methylcarbo[6]helicene (**6H$_{Me}$**) and 2-bromocarbo[6]helicene (**6H$_{Br}$**) were prepared through classic Wittig-reaction, followed by oxidative photocyclization (see the Supplementary Materials for synthetic details) (*43, 44*). When these monosubstituted carbo[6]-helicenes were used in the electrochemical C-H functionalization, a mixture of different alkoxylated products were obtained with total yields of 71 and 74% for **6H$_{Me}$-OMe** (**10**) and **6H$_{Br}$-OMe** (**11**), respectively. NMR of the combined products showed that the alkoxylation took place either on position-B2 or position-E1 (B2 is the antipode of E1), and no obvious selectivity was observed between these two positions. Hetero[6]helicenes including aza[6]helicene (**6H$_{aza}$**) and thia[6]helicene (**6H$_{thia}$**) were also synthesized and evaluated for the electrochemical C-H functionalization (Fig. 2C). **6H$_{aza}$** was alkoxylated on B2 or E1 with yields of 34% (**12a**) and 40% (**12b**), respectively. For **6H$_{thia}$**, the methoxy group was only installed on E1 (**13**), probably because of the specific geometry and relatively electron-donating feature of the five-member thiophene ring.

Longer carbo[n]helicenes (n = 7, 8, and 9; **7H**, **8H**, and **9H**) were also used for electrochemical C-H functionalization (Fig. 3A). **7H**, **8H**, and **9H** all gave mono-methoxylated products (**14** to **16**) in 74, 70, and 61% isolated yields, respectively. The methoxy groups all furnished on E1 of these carbo[n]helicenes as indicated by single-crystal x-ray diffraction (Fig. 3A, right). Apparently, such
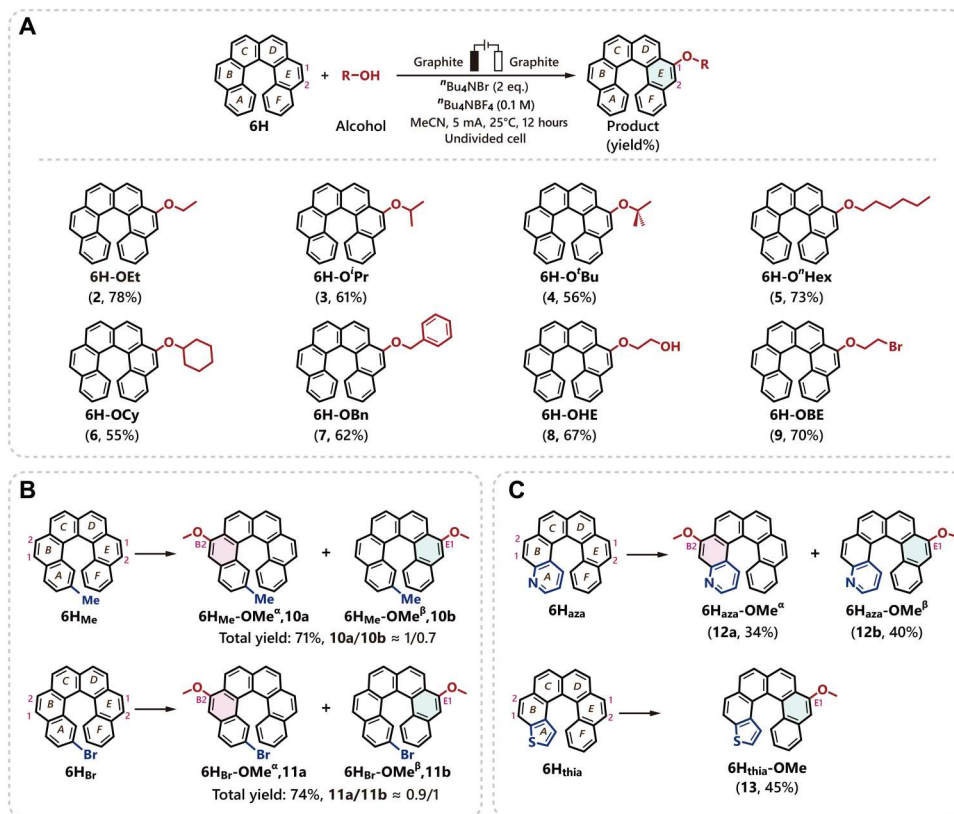
Fig. 2. Scope of electrochemical C-H functionalization of helicenes. (**A**) Electrochemical C-H functionalization of carbo[6]helicene with various alcohols. (**B**) Electrochemical C-H functionalization of substituted carbo[6]helicenes. (**C**) Electrochemical C-H functionalization of hetero[6]helicenes. Reaction conditions: helicene (0.1 mmol), alcohol (10 eq.), ^{n}Bu$_4$NBr (2 eq.), ^{n}Bu$_4$NBF$_4$ (0.1 M), MeCN (10 ml), 25°C, 12 hours, 5 mA, and undivided cell. Yields are for isolated products. For clarity, the aromatic rings of helicene are labeled by capital characters, and the C-H bonds are labeled by Arabic numbers.

remarkable selectivity is not a consequence of conventional electronic or steric effect due to the lack of electro-directing elements or bulky substituents for these primitive carbo[n]helicenes. By further scrutinizing the stereochemical structures of the alkoxylated products, we found that the hydrogen on the first position of helicene A1 might be crucial for the reaction selectivity. Although A1 is distant from E1, geometrically, the helical skeleton of helicene creates a helical back-biting route to make A1 and E1 spatially close to each other, which might affect the electrochemical C-H functionalization.

To gain more insights, we subsequently prepared 1,14-dimethylcarbo[5]helicene 5H$_{2Me}$ and 1,16-dimethylcarbo[6]helicene 6H$_{2Me}$ with methyl groups substituted on A1 and the antipodal E4 or F4. Unexpectedly, the electrochemical methoxylation proceeded effectively with these helicene derivatives, giving solely mono-methoxylated products 5H$_{2Me}$-OMe and 6H$_{2Me}$-OMe (17 and 18) in 71 and 72% yields, respectively (Fig. 3B). Despite the absence of the aryl hydrogen on A1 (and the antipode), the methoxylation processes still revealed accurate regioselectivity, but the methoxylated position was shifted from E1 to D1. In these cases, analogous spatial back-biting environments were found to be set up by the methyl hydrogen (Fig. 3B, right). Besides, in the case of 6H$_{2Ph}$ in which phenyl groups were substituted on A1 and F4, the methoxylation precisely occurred on C1 (19) and also reflected a back-biting effect generated by the phenyl hydrogen. On the contrary, the selectivity of the

electrochemical alkoxylation deteriorated when starting from 1,16-difluorocarbo[6]helicene 6H$_{2F}$ without any back-biting hydrogens, resulting in a mixture of products alkoxylated on E1 (6H$_{2F}$-OMe$^\alpha$) and D1 (6H$_{2F}$-OMe$^\beta$) and some other inseparable species (Fig. 3C).

The above intriguing results unambiguously suggested a unique directing effect from the helical back-biting hydrogens during the electrochemical C-H functionalization process. To reveal the detailed mechanism, we further investigated the reaction by cyclic voltammetry. The cyclic voltammogram of 6H showed two oxidation peaks at +1.22 and +1.38 V (versus Ag/Ag$^+$; fig. S103), respectively, which could be referred to the first oxidation to radical cation 6H$^{•+}$, and the further oxidation to 6H^{2+}. With the addition of MeOH, the first oxidation peak of 6H was retained, but the second peak almost disappeared (fig. S103A), indicating that MeOH might associate with the first oxidation intermediate 6H$^{•+}$ and thus interrupt the subsequent second oxidation process. To demonstrate the involvement of the radical species 6H$^{•+}$ in the electrochemical reaction, a radical scavenger 2,2,6,6-tetramethylpiperidinooxy was added into the reaction. The alkoxylation completely failed, and the 6H precursor merely converted to 6H-OMe after 12 hours (fig. S105). The two oxidation peaks of 6H were well retained with the addition of ^{n}Bu$_4$NBr, which showed two oxidation peaks at +0.43 and +0.87 V (versus Ag/Ag$^+$; the oxidative species probably included Br$_3^-$ and Br$_2$ and were abbreviated as [Br]$^+$) (45, 46), respectively (fig. S103B). Again, with the coexistence of MeOH, only the first
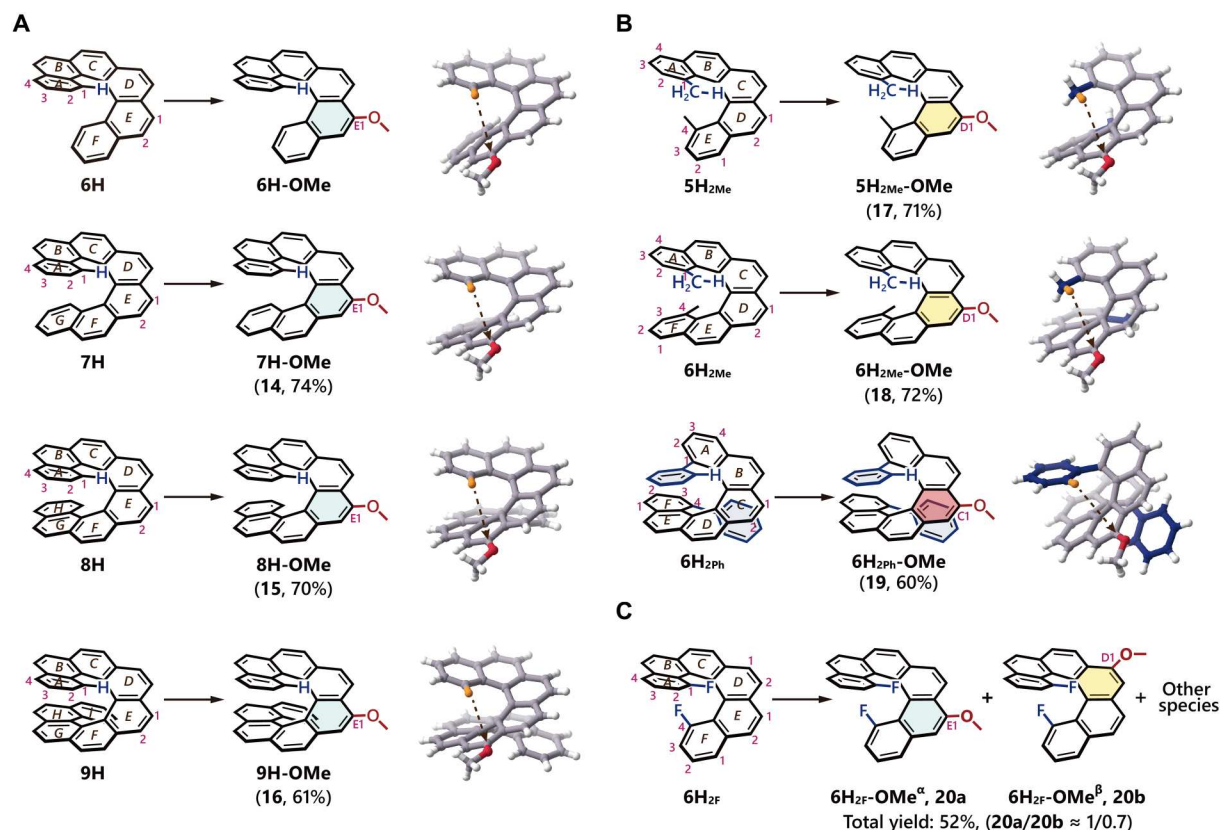
Fig. 3. Helicity-modulated hydrogen-directed regioselective electrochemical C-H functionalization of carbohelicenes. (**A**) Regioselective electrochemical C-H functionalization of carbo[7]helicene (**7H**), carbo[8]helicene (**8H**), and carbo[9]helicene (**9H**). Right: Single-crystal structures. (**B**) Back-biting methyl and phenyl hydrogen–directed regioselective electrochemical C-H functionalization of 1,14-dimethylcarbo[5]helicene (**5H$_{2Me}$**), 1,16-dimethylcarbo[6]helicene (**6H$_{2Me}$**), and 1,16-diphenyl-carbo[6]helicene (**6H$_{2Ph}$**). Right: Single-crystal structures. (**C**) Electrochemical C-H functionalization of 1,16-difluorocarbo[6]helicene (**6H$_{2F}$**) in the absence of helical back-biting hydrogen. Reaction conditions: helicene (0.1 mmol), MeOH (10 eq.), $^nBu_4NBr$ (2 eq.), $^nBu_4NBF_4$ (0.1 M), MeCN/CH$_2$Cl$_2$ (9/1, v/v, 10 ml; to promote the dissolution of longer helicenes and disubstituted helicenes, CH$_2$Cl$_2$ was added as a cosolvent), 25°C, 12 hours, 5 mA, and undivided cell. Yields are for isolated products. For clarity, the aromatic rings of helicenes are labeled by capital characters, and the C-H bonds are labeled by Arabic numbers.

oxidation peak of **6H** could be observed (fig. S103A). It has been noted above that the electrochemical C-H functionalization only proceeded with the presence of $^nBu_4NBr$ (Table 1). However, the oxidative species of Br^- (namely, $[Br]^+$) with lower oxidation potential were apparently incapable of directly oxidizing the **6H** precursor. This was further demonstrated by parallel experiments using Br_2 as the chemical oxidant, which failed to convert **6H** into any detectable products after 12 hours (fig. S105). Consequently, it seemed that the in situ generated $[Br]^+$ probably interacted with the intermediate formed by **6H$^{•+}$** and MeOH.

In consideration of the above results, we proposed a reaction mechanism involving helical back-biting hydrogen−directed remote C-H functionalization with the assistance of theoretical calculations, which was carried out using the Gaussian 09 program [program at the M06-2X-D3/def2-TZVPD//PBE0-D3(BJ)/def2-SVP level of theory with the SMD continuum solvent model (Fig. 4A)] (47–49). First, **6H** is electrochemically oxidized on the anode, giving a radical cation **6H$^{•+}$**. The calculated oxidation potential is +1.79 V versus standard hydrogen electrode (SHE) (+1.20 V versus Ag/Ag$^+$), which is well consistent with the cyclic voltammetry (CV) result. Then, **6H$^{•+}$** attracts one MeOH molecule and forms a complex **[6H••MeOH]$^{•+}$**. The MeOH molecule is found to be

anchored on the groove of helicene in this intermediate. Typically, the oxygen atom of MeOH shows a relatively short distance of 2.19 Å to the hydrogen at A1 (H$_{A1}$) and 3.01 Å to the π-surface of helicene (Fig. 4B(I), generating a unique helical back-biting environment. According to the noncovalent interaction (NCI) analysis (50), the O••H$_{A1}$ interaction gives an obvious hydrogen-bonding character [Sign(λ_2)ρ = −0.17, in blue], while the O••π interaction is more like van der Waals interaction [Sign(λ_2)ρ ~ 0, in green; Fig. 4B (I), and figs. S115 and S116]. Such complexation reveals a relatively high binding energy (ΔH_{calc}) of 3.2 kcal mol^{-1}, resulting in a fairly stable intermediate. Notably, the position of the oxygen atom is approximately on the top of E1. Later, **[6H••MeOH]$^{•+}$** undergoes proton elimination, giving a neutral radical species **[6H••OMe]$^•$**. This neutral intermediate also shows a similar complexation conformation with obvious hydrogen-bonding between oxygen and H$_{A1}$ [Sign(λ_2)ρ = −0.12, in blue], along with van der Waals interaction between oxygen and the π-surface [Fig. 4B (II) and figs. S117 and S118]. Subsequently, the oxygen attacks the adjacent carbon at E1 to afford a covalent species **[6H-OMe]$^•$** via a transition state **[6H••OMe]$^{•‡}$** with an activation free-energy $\Delta G^{‡}_{calc}$ of +11.5 kcal mol^{-1}. Notably, when scrutinizing this transformation, we found how this nontrivial hydrogen bonding assisted
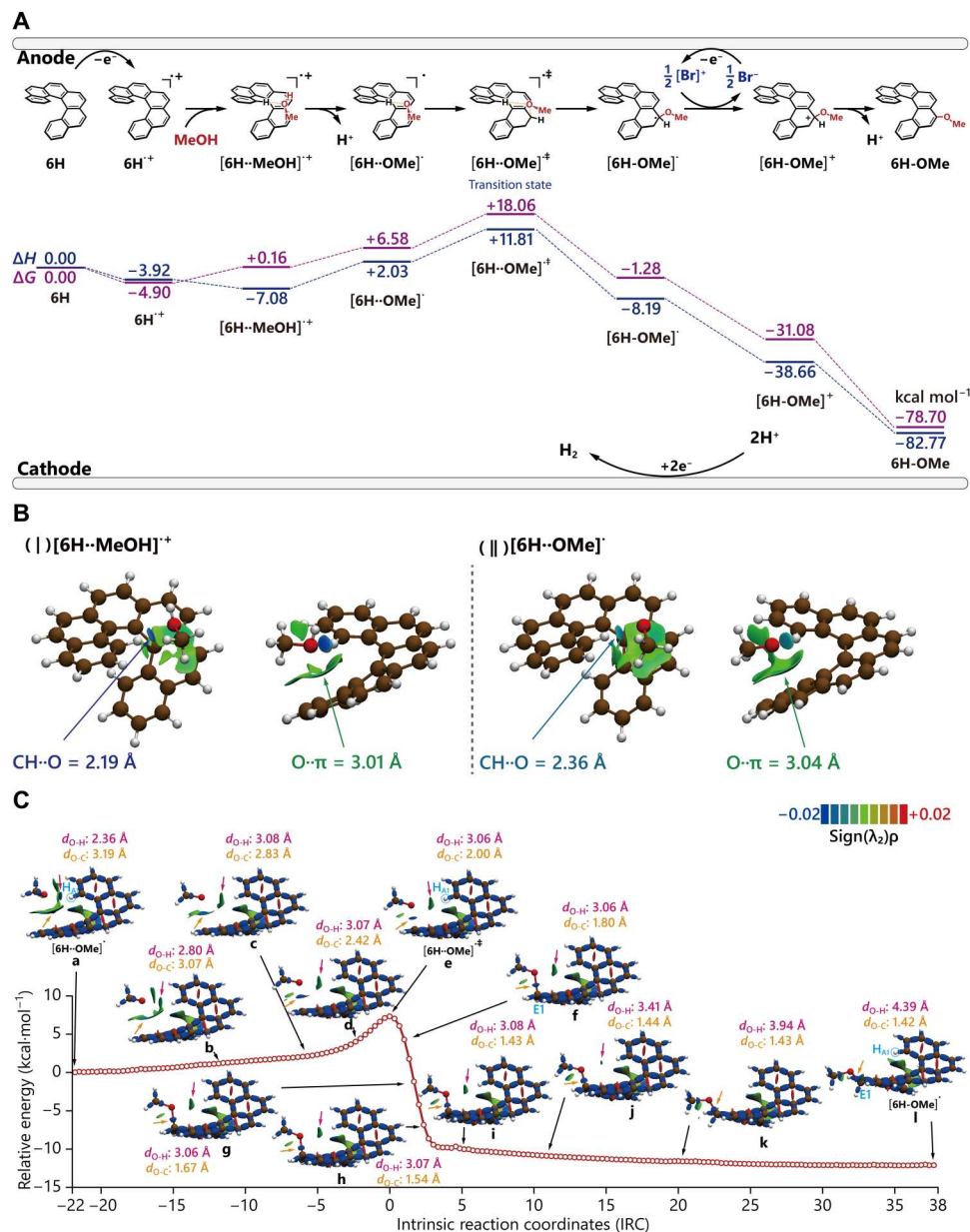
Fig. 4. Mechanism study on helical back-biting hydrogen-directed C-H functionalization. (**A**) Reaction pathway for electrochemical remote C-H functionalization of **6H**. (**B**) Noncovalent interaction (NCI) maps of intermediates [**6H··MeOH**]$^{•+}$ and [**6H··OMe**]$^{•}$. (**C**) IRI maps at representative points of an IRC path from [**6H··OMe**]$^{•}$ to [**6H-OMe**]$^{•}$ via a transition state [**6H··OMe**]$^{•‡}$. Density functional theory calculations of the thermal energies (ΔH and ΔG) and the NCI map and IRI map were performed at the M06-2X-D3/def2-TZVPD//PBE0-D3(BJ)/def2-SVP level of theory; the relative energy refers to the electronic energy calculated by IRC at the PBE0-D3(BJ)/def2-SVP level of theory.

the regioselective C-O bond formation. Figure 4C illustrated the interaction region indicator (IRI) maps (51) at representative points of an intrinsic reaction coordinate (IRC) path from [**6H··OMe**]$^{•}$ to [**6H-OMe**]$^{•}$. At the first stage (**a** to **c**), the methoxy starts to attack the corresponding carbon atom by shortening the O-C bond (from 3.19 to 2.83 Å) and elongating the O-H bond (from 2.36 to 3.08 Å). In this stage, the hydrogen bonding is weakened, while the O··π interaction is enhanced and becomes more localized above C_{E1}. For the second stage (**c** to **i**), this moderate hydrogen bonding keeps its intensity with nearly no change of the distance (ca. 3.07 Å), while the C-O bond is further enhanced, becoming a covalent

bond (from 2.83 to 1.43 Å) by passing the energy barrier. Then, the last stage (**i** to **l**) shows the cutoff of the hydrogen bond by further increasing the distance, and the molecule adjusts the geometry to a more stable form. Afterward, [**6H-OMe**]$^{•}$ takes a second oxidation to form cationic [**6H-OMe**]$^{+}$ with a relatively low calculated oxidation potential of +0.71 V versus SHE (+0.12 V versus Ag/Ag^{+}), which might be promoted by the oxidative species ([Br]$^{+}$) of Br^{-}. Last, the following deprotonation process gives the neutral product **6H-OMe**. In general, **6H** sequentially undergoes electrooxidation and deprotonation to form the alkoxylated product,

and the accurate functionalization is substantially achieved by the back-biting–fashioned complexation between MeOH and helicene.

Such regioselective remote C-H functionalization provided a feasible approach to finely tune the optical properties of PAHs. To this end, we prepared a pair of methoxy-substituted *N*-methylated aza[6]helicene, namely, cationic **6H$_{aza}^+$-OMe$^\alpha$** and **6H$_{aza}^+$-OMe$^\beta$**, by sequential C-H methoxylation and *N*-methylation of **6H$_{aza}$** (Fig. 5A). Compared with neutral **6H$_{aza}$-OMe**, the cationic **6H$_{aza}^+$-OMe** products showed red-shifted absorption and luminescence spectra (Fig. 5A), indicating a push-pull effect in the helical system. The luminescence of **6H$_{aza}^+$-OMe$^\beta$** with the methoxy group

located distant to the nitrogen atom altered severely in different solvents, namely, blue ($\lambda_{max} = 458$ nm) in tetrahydrofuran (THF), light blue ($\lambda_{max} = 502$ nm) in dimethyl sulfoxide (DMSO), yellow ($\lambda_{max} = 563$ nm) in MeOH, and orange ($\lambda_{max} = 630$ nm) in dichloromethane (DCM), while **6H$_{aza}^+$-OMe$^\alpha$** with the methoxy group close to the nitrogen atom constantly gave yellowish green emission ($\lambda_{max} = 510$ to 527 nm). The frontier molecular orbitals (MOs) in **6H$_{aza}^+$-OMe$^\alpha$** and **6H$_{aza}^+$-OMe$^\beta$** were consistent with the push-pull character. The occupied MOs span over the domain distant to the nitrogen atom, while the unoccupied MOs are centered at the aromatic rings close to the nitrogen atom (Fig. 5B). According to the
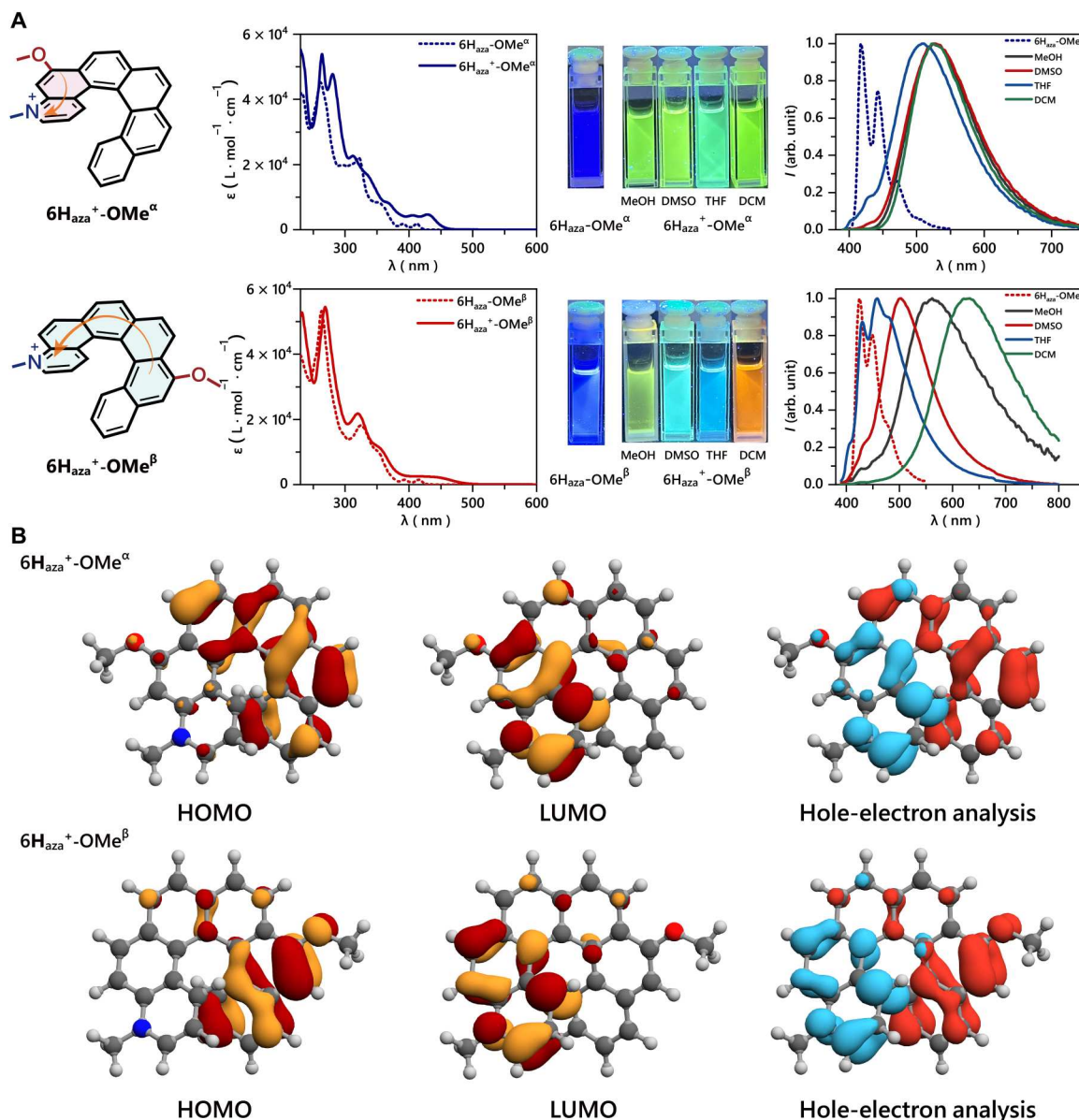

Fig. 5. Regioselective methoxylation of *N*-methylated aza[6]helicene and modulation of solvent-dependent luminescence. (**A**) Chemical structures of **6H$_{aza}^+$-OMe$^\alpha$** and **6H$_{aza}^+$-OMe$^\beta$**; ultraviolet-visible absorption spectra of **6H$_{aza}$-OMe$^\alpha$** and **6H$_{aza}$-OMe$^\beta$** (in DCM, $c = 2.0 \times 10^{-5}$ M) and **6H$_{aza}^+$-OMe$^\alpha$** and **6H$_{aza}^+$-OMe$^\beta$** (in MeOH, $c = 2.0 \times 10^{-5}$ M); photographs of corresponding solutions in different solvents recorded under irradiation at 365 nm; and fluorescence spectra of **6H$_{aza}^+$-OMe$^\alpha$** and **6H$_{aza}^+$-OMe$^\beta$** in MeOH, DMSO, THF, and DCM ($c = 2.0 \times 10^{-5}$ M). (**B**) Isosurfaces of frontier MOs of **6H$_{aza}^+$-OMe$^\alpha$** and **6H$_{aza}^+$-OMe$^\beta$** and hole-electron analysis of **6H$_{aza}^+$-OMe$^\alpha$** and **6H$_{aza}^+$-OMe$^\beta$**. HOMO, highest occupied molecular orbital; LUMO, lowest unoccupied molecular orbital.

hole-electron analysis on the first excited state using Multiwfn 3.8-dev program (*52*, *53*), we find that *D* index (the distance between the centroid of the hole and the centroid of the electron) is 2.5 Å for $6H_{aza}^+$-OMe^α and 3.8 Å for $6H_{aza}^+$-OMe^β for transition $S_1 \rightarrow S_0$. Besides, for this transition, the S_r index (overlapping degree between hole and electron; 0 for perfect overlapping and 1 for non-overlapping) is 0.34 arbitrary units (a.u.) for $6H_{aza}^+$-OMe^α and 0.58 a.u. for $6H_{aza}^+$-OMe^β, indicating a higher degree of separation between the hole and electron in $6H_{aza}^+$-OMe^β (Fig. 5B). Thus, for transition $S_1 \rightarrow S_0$, $6H_{aza}^+$-OMe^β shows a higher degree of charge transfer than $6H_{aza}^+$-OMe^α, which might be more affected by the solvent environment, causing the diverse color change in different solvents (*54–56*).

In conclusion, we have developed a facile helicity-modulated metal/template-free electrochemical remote C-H functionalization method for accurate alkoxylation of helical PAHs with remarkable regioselectivity. A rich array of alkoxy groups have been precisely attached to the helical backbone of various helicenes, which is directed by the aromatic or aliphatic hydrogen through a helical back-biting path. The back-biting aromatic or aliphatic hydrogens associate with the alcohol substrates via hydrogen bonding and direct the installation of alkoxy groups at the opposite position of the helical skeleton. The precise modification also provides an approach to modulate the electronic and optical properties of helicenes. We believe that such distinctive helicity-modulated hydrogen-directed C-H functionalization would be prevalent in other molecule systems as long as a back-biting environment exists. Specifically, we are currently exploring a broad array of helicenes and nonplanar nanographenes (*57*, *58*), aiming at a feasible portal to direct C-H functionalization of complex arenes. We are also preparing a series of laterally extendable helicene ligands using this method for designed association, polymerization, and grafting of covalent or coordinating chiral molecular cages (*59*, *60*).

MATERIALS AND METHODS
General procedure for the helicity-modulated H-directed electrochemical C-H functionalization
Helicene substrate (0.1 mmol) was dissolved in 10 ml of dried MeCN containing 0.1 M $^nBu_4NBF_4$ as the electrolyte in an undivided cell. Alcohol (10 eq.) and 2 eq. of $^nBu_4NBr$ were added into the solution. The reaction mixture was electrolyzed at room temperature under a constant current of 5 mA for 12 hours. After the reaction, 50 ml of water was added, and the mixture was extracted by 50 ml of CH_2Cl_2 twice. The organic layers were combined, dried over $MgSO_4$, and concentrated under vacuum. The residue was purified by silica thin-layer chromatography using a mixed solvent of heptane and CH_2Cl_2 as the eluent to afford the alkoxylated products. The synthesis of helical starting materials is depicted in detail in the Supplementary Materials.

Supplementary Materials
This PDF file includes:
Supplementary Text
Figs. S1 to S142
Tables S1 to S16

REFERENCES AND NOTES
1. K. Godula, D. Sames, C-H bond functionalization in complex organic synthesis. *Science* **312**, 67–72 (2006).
2. W. R. Gutekunst, P. S. Baran, C-H functionalization logic in total synthesis. *Chem. Soc. Rev.* **40**, 1976–1991 (2011).
3. J. Yamaguchi, A. D. Yamaguchi, K. Itami, C-H bond functionalization: Emerging synthetic tools for natural products and pharmaceuticals. *Angew. Chem. Int. Ed.* **51**, 8960–9009 (2012).
4. D. J. Abrams, P. A. Provencher, E. J. Sorensen, Recent applications of C-H functionalization in complex natural product synthesis. *Chem. Soc. Rev.* **47**, 8925–8967 (2018).
5. H. M. L. Davies, J. Du Bois, J.-Q. Yu, C-H functionalization in organic synthesis. *Chem. Soc. Rev.* **40**, 1855–1856 (2011).
6. H. M. L. Davies, D. Morton, Collective approach to advancing C-H functionalization. *ACS Cent. Sci.* **3**, 936–943 (2017).
7. B. Galabov, D. Nalbantova, P. v. R. Schleyer, H. F. Schaefer III, Electrophilic aromatic substitution: New insights into an old class of reactions. *Acc. Chem. Res.* **49**, 1191–1199 (2016).
8. J. Mortier, *Arene Chemistry: Reaction Mechanisms and Methods for Aromatic Compounds* (Wiley, 2016).
9. M. M. Heravi, V. Zadsirjan, P. Saedi, T. Momeni, Applications of Friedel-Crafts reactions in total synthesis of natural products. *RSC Adv.* **8**, 40061–40163 (2018).
10. L. Ackermann, N. Hofmann, R. Vicente, Carboxylate-assisted ruthenium-catalyzed direct alkylations of ketimines. *Org. Lett.* **13**, 1875–1877 (2011).
11. T. Gensch, M. N. Hopkinson, F. Glorius, J. Wencel-Delord, Mild metal-catalyzed C-H activation: Examples and concepts. *Chem. Soc. Rev.* **45**, 2900–2936 (2016).
12. C. Sambiagio, D. Schönbauer, R. Blieck, T. Dao-Huy, G. Pototschnig, P. Schaaf, T. Wiesinger, M. F. Zia, J. Wencel-Delord, T. Besset, B. U. W. Maes, M. Schnürch, A comprehensive overview of directing groups applied in metal-catalysed C-H functionalisation chemistry. *Chem. Soc. Rev.* **47**, 6603–6743 (2018).
13. J. Loup, U. Dhawa, F. Pesciaioli, J. Wencel-Delord, L. Ackermann, Enantioselective C-H activation with earth-abundant 3d transition metals. *Angew. Chem. Int. Ed.* **58**, 12803–12818 (2019).
14. X. Chen, K. M. Engle, D.-H. Wang, J.-Q. Yu, Palladium(II)-catalyzed C-H activation/C-C cross-coupling reactions: Versatility and practicality. *Angew. Chem. Int. Ed.* **48**, 5094–5115 (2009).
15. S. R. Neufeldt, M. S. Sanford, Controlling site selectivity in palladium catalyzed C-H bond functionalization. *Acc. Chem. Res.* **45**, 936–946 (2012).
16. U. Dutta, S. Maiti, T. Bhattacharya, D. Maiti, Arene diversification through distal C(sp²)-H functionalization. *Science* **372**, eabd5992 (2021).
17. D. Leow, G. Li, T.-S. Mei, J.-Q. Yu, Activation of remote *meta*-C-H bonds assisted by an end-on template. *Nature* **486**, 518–522 (2012).
18. X.-C. Wang, W. Gong, L.-Z. Fang, R.-Y. Zhu, S. Li, K. M. Engle, J.-Q. Yu, Ligand-enabled *meta*-C-H activation using a transient mediator. *Nature* **519**, 334–338 (2015).
19. Y. Kuninobu, H. Ida, M. Nishi, M. Kanai, A *meta*-selective C-H borylation directed by a secondary interaction between ligand and substrate. *Nat. Chem.* **7**, 712–717 (2015).
20. Z. Zhang, K. Tanaka, J.-Q. Yu, Remote site-selective C-H activation directed by a catalytic bifunctional template. *Nature* **543**, 538–542 (2017).
21. K. Ramakrishna, J. P. Biswas, S. Jana, T. K. Achar, S. Porey, D. Maiti, Coordination assisted distal C-H alkylation of fused heterocycles. *Angew. Chem. Int. Ed.* **58**, 13808–13812 (2019).
22. Y. Segawaa, D. W. Stephan, Metal-free hydrogenation catalysis of polycyclic aromatic hydrocarbons. *Chem. Commun.* **48**, 11963–11965 (2012).
23. M. N. Eliseeva, L. T. Scott, Pushing the Ir-catalyzed C-H polyborylation of aromatic compounds to maximum capacity by exploiting reversibility. *J. Am. Chem. Soc.* **134**, 15169–15172 (2012).
24. R. P. Kaiser, J. Ulč, I. Císařová, D. Nečas, Direct regioselective C-H borylation of [5]helicene. *RSC Adv.* **8**, 580–583 (2018).
25. Y. Shen, C.-F. Chen, Helicenes: Synthesis and applications. *Chem. Rev.* **112**, 1463–1535 (2012).
26. M. Gingras, One hundred years of helicene chemistry. Part 1: Non-stereoselective syntheses of carbohelicenes. *Chem. Soc. Rev.* **42**, 968–1006 (2013).
27. K. Dhbaibi, L. Favereau, J. Crassous, Enantioenriched helicenes and helicenoids containing main-group elements (B, Si, N, P). *Chem. Rev.* **119**, 8846–8953 (2019).
28. H. Lund, A century of organic electrochemistry. *J. Electrochem. Soc.* **149**, S21–S33 (2002).
29. R. Francke, R. D. Little, Redox catalysis in organic electrosynthesis: Basic principles and recent developments. *Chem. Soc. Rev.* **43**, 2492–2521 (2014).
30. A. Wiebe, T. Gieshoff, S. Möhle, E. Rodrigo, M. Zirbes, S. R. Waldvogel, Electrifying organic synthesis. *Angew. Chem. Int. Ed.* **57**, 5594–5619 (2018).
31. P. Xiong, H.-C. Xu, Chemistry with electrochemically generated *N*-centered radicals. *Acc. Chem. Res.* **52**, 3339–3350 (2019).

32. M. D. Kärkäs, Electrochemical strategies for C–H functionalization and C–N bond formation. *Chem. Soc. Rev.* **47**, 5786–5865 (2018).

33. N. Sauermann, T. H. Meyer, Y. Qiu, L. Ackermann, Electroactalytic C–H activation. *ACS Catal.* **8**, 7086–7103 (2018).

34. K.-J. Jiao, Y.-K. Xing, Q.-L. Yang, H. Qiu, T.-S. Mei, Site-selective C–H functionalization *via* synergistic use of electrochemistry and transition metal catalysis. *Acc. Chem. Res.* **53**, 300–310 (2020).

35. X. Gao, P. Wang, L. Zeng, S. Tang, A. Lei, Cobalt(II)-catalyzed electrooxidative C–H amination of arenes with alkylamines. *J. Am. Chem. Soc.* **140**, 4195–4199 (2018).

36. U. Dhawa, C. Tian, T. Wdowik, J. C. A. Oliveira, J. Hao, L. Ackermann, Enantioselective pallada-electrocatalyzed C–H activation by transient directing groups: Expedient access to helicenes. *Angew. Chem. Int. Ed.* **59**, 13451–13457 (2020).

37. M. S. H. Salem, M. I. Khalid, M. Sako, K. Higashida, C. Lacroix, M. Kondo, R. Takishima, T. Taniguchi, M. Miura, G. Vo-Thanh, H. Sasai, S. Takizawa, Electrochemical synthesis of hetero[7]helicene containing pyrrole and furan rings *via* an oxidative heterocoupling and dehydrative cyclization sequence. *Adv. Synth. Catal.* **365**, 373–380 (2023).

38. Q. Zhu, C. Kan, Y. Cao, Z. Tang, K. Xu, P. Hang, B. Li, Y. Yao, M. Lei, X. Yu, Tandem electro-oxidative C–C and C–N coupling and aromatization for the construction of pyrazine-fused bis - aza[7]helicene. *Org. Lett.* **24**, 7053–7057 (2022).

39. J. Vacek, J. Zadny, J. Storch, J. Hrbac, Chiral electrochemistry: Anodic deposition of enantiopure helical molecules. *ChemPlusChem* **85**, 1954–1958 (2020).

40. M. Jakubec, T. Beránek, P. Jakubík, J. Sýkora, J. Žádný, V. Církva, J. Storch, 2-Bromo[6]helicene as a key intermediate for [6]helicene functionalization. *J. Org. Chem.* **83**, 3607–3616 (2018).

41. M. Jakubec, J. Storch, Recent advances in functionalizations of helicene backbone. *J. Org. Chem.* **85**, 13415–13428 (2020).

42. M. Jakubec, I. Ghosh, J. Storch, B. König, Photochemical functionalization of helicenes. *Chem. A Eur. J.* **26**, 543–547 (2020).

43. Y. Nakai, T. Mori, Y. Inoue, Theoretical and experimental studies on circular dichroism of carbo[*n*]helicenes. *J. Phys. Chem. A* **116**, 7372–7385 (2012).

44. F. B. Mallory, C. W. Mallory, *Photocyclization of Stilbenes and Related Molecules* (Wiley, 1984).

45. K. Mitsudo, R. Matsuo, T. Yonezawa, H. Inoue, H. Mandai, S. Suga, Electrochemical synthesis of thienoacene derivatives: Transition-metal-free dehydrogenative C–S coupling promoted by a halogen mediator. *Angew. Chem. Int. Ed.* **59**, 7803–7807 (2020).

46. T. Takiguchi, T. Nonaka, Influence of Br⁻ concentration on (Br)⁺-mediated indirect electrooxidation of alcohols to the corresponding carbonyl compounds. *Bull. Chem. Soc. Jpn.* **60**, 3137–3142 (1987).

47. C. Adamo, V. Barone, Toward reliable density functional methods without adjustable parameters: The PBE0 model. *J. Chem. Phys.* **110**, 6158–6170 (1999).

48. S. Grimme, J. Antony, S. Ehrlich, H. Krieg, A consistent and accurate ab initio parametrization of density functional dispersion correction (DFT-D) for the 94 elements H-Pu. *J. Chem. Phys.* **132**, 154104 (2010).

49. F. Weigend, R. Ahlrichs, Balanced basis sets of split valence, triple zeta valence and quadruple zeta valence quality for H to Rn: Design and assessment of accuracy. *Phys. Chem. Chem. Phys.* **7**, 3297–3305 (2005).

50. J. Contreras-García, E. R. Johnson, S. Keinan, R. Chaudret, J. -P. Piquemal, D. N. Beratan, W. T. Yang, NCIPLOT: A program for plotting noncovalent interaction regions. *J. Chem. Theory. Comput.* **7**, 625–632 (2011).

51. T. Lu, Q. X. Chen, Interaction region indicator: A simple real space function clearly revealing both chemical bonds and weak interactions. *Chemistry-Methods* **1**, 231–239 (2021).

52. Z. Y. Liu, T. Lu, Q. X. Chen, An sp-hybridized all-carboatomic ring, cyclo[18]carbon: Bonding character, electron delocalization, and aromaticity. *Carbon* **165**, 468–475 (2020).

53. T. Lu, F. W. Chen, Multiwfn: A multifunctional wavefunction analyzer. *J. Comput. Chem.* **33**, 580–592 (2012).

54. K. Dhbaibi, L. Favereau, M. Srebro-Hooper, C. Quinton, N. Vanthuyne, L. Arrico, T. Roisnel, B. Jamoussi, C. Poriel, C. Cabanetos, J. Autschbach, J. Crassous, Modulation of circularly polarized luminescence through excited-state symmetry breaking and interbranched exciton coupling in helical push-pull organic systems. *Chem. Sci.* **11**, 567–576 (2020).

55. Z. H. Zhao, M. Y. Zhang, D. H. Liu, C. H. Zhao, Modification of [5]helicene with dimesitylboryl: One way to enhance the fluorescence efficiency. *Org. Lett.* **20**, 7590–7593 (2018).

56. A. Marini, A. Muñoz-Losa, A. Biancardi, B. Mennucci, What is solvatochromism? *J. Phys. Chem. B* **114**, 17128–17135 (2010).

57. C. S. Shen, G. L. Zhang, Y. L. Ding, N. Yang, F. W. Gan, J. Crassous, H. B. Qiu, Oxidative cyclo-rearrangement of helicenes into chiral nanographenes. *Nat. Commun.* **12**, 2786 (2021).

58. J. H. Wang, C. S. Shen, G. L. Zhang, F. W. Gan, Y. L. Ding, H. B. Qiu, Transformation of crowded oligoarylene into perylene-cored chiral nanographene by sequential oxidative cyclization and 1,2-phenyl migration. *Angew. Chem. Int. Ed.* **61**, e202115979 (2022).

59. A. U. Malik, F. W. Gan, C. S. Shen, N. Yu, R. B. Wang, J. Crassous, M. H. Shu, H. B. Qiu, Chiral organic cages with a triple-stranded helical structure derived from helicene. *J. Am. Chem. Soc.* **140**, 2769–2772 (2018).

60. Y. L. Ding, C. S. Shen, F. W. Gan, J. H. Wang, G. L. Zhang, L. L. Li, M. H. Shu, B. S. Zhu, J. Crassous, H. B. Qiu, Tunable construction of transition metal-coordinated helicene cages. *Chinese Chem. Lett.* **32**, 3988–3992 (2021).